Evaluation of iron overload in nigrosome 1 via quantitative susceptibility mapping as a progression biomarker in prodromal stages of synucleinopathies

Marta Lancione [a,b,1], Graziella Donatelli [b,c,1,*], Eleonora Del Prete [d], Nicole Campese [d], Daniela Frosini [d], Matteo Cencini [a,b], Mauro Costagli [a,e], Laura Biagi [a,b], Giacomo Lucchi [f], Michela Tosetti [a,b], Massimiliano Godani [g], Dario Arnaldi [e,h], Michele Terzaghi [i,j], Federica Provini [k,l], Claudio Pacchetti [m], Pietro Cortelli [k,l], Enrica Bonanni [d], Roberto Ceravolo [d], Mirco Cosottini [f]

[a] Laboratory of Medical Physics and Magnetic Resonance, IRCCS Stella Maris, Pisa, Italy
[b] Imago7 Research Foundation, Pisa, Italy
[c] Neuroradiology Unit, Azienda Ospedaliero-Universitaria Pisana, Pisa, Italy
[d] Neurology Unit, Department of Clinical and Experimental Medicine, University of Pisa, Pisa, Italy
[e] Department of Neuroscience, Rehabilitation, Ophthalmology, Genetics, Maternal and Child Sciences (DINOGMI), University of Genoa, Genoa, Italy
[f] Neuroradiology Unit, Department of Translational Research on New Technologies in Medicine and Surgery, University of Pisa, Pisa, Italy
[g] Neurology Unit, Sant'Andrea Hospital, La Spezia, Italy
[h] IRCCS Ospedale Policlinico San Martino, Genoa, Italy
[i] Department of Brain and Behavioral Sciences, University of Pavia, Pavia, Italy
[j] IRCCS Mondino Foundation, Pavia, Italy
[k] IRCCS Istituto delle Scienze Neurologiche di Bologna, Clinica Neurologica Rete Metropolitana, Bologna, Italy
[l] Department of Biomedical and Neuromotor Sciences (DIBINEM), University of Bologna, Bologna, Italy
[m] Parkinson's Disease and Movement Disorders Unit, IRCCS Mondino Foundation, Pavia, Italy

ARTICLE INFO

ABSTRACT

Idiopathic rapid eye movement (REM) sleep behavior disorder (iRBD) is a prodromal stage of α-synucleinopathies, such as Parkinson's disease (PD), which are characterized by the loss of dopaminergic neurons in substantia nigra, associated with abnormal iron load. The assessment of presymptomatic biomarkers predicting the onset of neurodegenerative disorders is critical for monitoring early signs, screening patients for neuroprotective clinical trials and understanding the causal relationship between iron accumulation processes and disease development. Here, we used Quantitative Susceptibility Mapping (QSM) and 7T MRI to quantify iron deposition in Nigrosome 1 (N1) in early PD (ePD) patients, iRBD patients and healthy controls and investigated group differences and correlation with disease progression. We evaluated the radiological appearance of N1 and analyzed its iron content in 35 ePD, 30 iRBD patients and 14 healthy controls via T2*-weighted sequences and susceptibility (χ) maps. N1 regions of interest (ROIs) were manually drawn on control subjects and warped onto a study-specific template to obtain probabilistic N1 ROIs. For each subject the N1 with the highest mean χ was considered for statistical analysis. The appearance of N1 was rated pathological in 45% of iRBD patients. ePD patients showed increased N1 χ compared to iRBD patients and HC but no correlation with disease duration, indicating that iron load remains stable during the early stages of disease progression. Although no difference was reported in iron content between iRBD and HC, N1 χ in the iRBD group increases as the disease evolves. QSM can reveal temporal changes in N1 iron content and its quantification may represent a valuable presymptomatic biomarker to assess neurodegeneration in the prodromal stages of PD.

1. Introduction

Parkinson's Disease (PD) is a progressive and disabling neurodegenerative disease with a higher prevalence in elderly people, characterized by striatal dopamine deficiency and motor symptoms as bradykinesia plus muscular rigidity and/or rest tremor (Postuma et al., 2015a). Pathological hallmarks of the disease are the loss of dopaminergic neurons, mainly in substantia nigra (SN) pars compacta (SNc), and the accumulation of intra-cytoplasmic Lewy bodies inclusions containing misfolded α-synuclein (Fearnley and Lees, 1991; Gibb and Lees, 1988; Spillantini et al., 1998). Evidence suggests that these pathological changes appear years before the onset of symptoms (Fearnley and Lees, 1991; Gibb and Lees, 1988) and that 68% of dopaminergic neurons of the ventrolateral tier of the SNc are lost at the time of clinical onset (Fearnley and Lees, 1991).

Current medical therapies aim to treat motor symptoms mainly by restoring the striatal dopamine levels, whereas treatments to prevent, halt or slow the rate of disease progression are not yet available (Balestrino and Schapira, 2020). The future availability of neuroprotective and disease-modifying drugs would represent a milestone in the pharmacological treatment of PD. In this context, the presymptomatic phase of PD is of huge relevance in the search for biomarkers of neurodegeneration occurrence and of forthcoming phenoconversion (Postuma et al., 2015b).

Recently, the idiopathic rapid eye movement (REM) sleep behavior disorder (iRBD), a parasomnia characterized by loss of muscular atonia during REM sleep and dream enacting behaviors (Schenck et al., 1986), has been recognized as a prodromal condition of synucleinopathies (Galbiati et al., 2019). Polysomnography-confirmed iRBD has a pooled prevalence of 0.68% (Cicero et al., 2021) and patients have an increased risk of developing parkinsonism compared to control populations (Yao et al., 2021). PD and Dementia with Lewy Bodies (DLB) are the most common phenoconversion diagnosis of iRBD patients, with the overall risk for neurodegeneration increasing over time and reaching 96.6% at 14 years follow-up (Galbiati et al., 2019).

Together with Lewy body inclusions and dopaminergic neuronal loss, iron accumulation in the SNc is another hallmark of the neuropathology of PD (Jellinger et al., 1990; Sofic et al., 1991). The iron overload can be visible as T2* hypointensity and estimated using Quantitative Susceptibility Mapping (QSM) (Barbosa et al., 2015; Costagli et al., 2016; He et al., 2015; Langkammer et al., 2012; Sun et al., 2015), thus representing a potentially valuable marker in motor and premotor stages of synucleinopathies.

In the last decade the Nigrosome 1 (N1), an ovoid shape area corresponding to the ventrolateral tier of SNc, was described as abnormally hypointense in T2*-weighted images in most PD patients (Blazejewska et al., 2013; Cosottini et al., 2015, 2014) and in a variable share of iRBD patients (Barber et al., 2020; De Marzi et al., 2016; Frosini et al., 2017). The abnormal nigral iron storage has also been documented and estimated using QSM assessing altered susceptibility (χ) in the whole SN (An et al., 2018; Barbosa et al., 2015; Langkammer et al., 2016; Murakami et al., 2015; Sun et al., 2020), in the SN pars reticulata (Chen et al., 2019; Du et al., 2018; Xuan et al., 2017) and in the SN pars compacta (Barbosa et al., 2015; Chen et al., 2019; Du et al., 2018; Takahashi et al., 2018b; Xuan et al., 2017), but without purposely targeting N1.

Recent studies showed that most iRBD patients with N1 hypointensity have dopamine transporter single photon emission tomography (123I-FP-CIT SPECT) evidence of nigro-striatal dysfunction (Bae et al., 2018; Barber et al., 2020; Frosini et al., 2017) and thus are at higher risk of forthcoming phenoconversion (Iranzo et al., 2017, 2010). Therefore, MRI could represent a useful tool for improving our insight into the presymptomatic stage of PD and N1 abnormality may be a marker for short-term risk of overt synucleinopathy occurrence in iRBD patients (Bae et al., 2018).

Here we employed QSM at ultra-high magnetic field to investigate differences in N1 iron deposition between early PD patients (ePD), iRBD patients and healthy controls, and between specific subgroups of patients. Then, we explored the association between N1 iron accumulation and disease duration in both iRBD and ePD patients.

2. Methods

2.1. Subjects

Patients with a diagnosis of PD or iRBD were clinically evaluated and recruited at the Movement Disorders Center of the University of Pisa during the period 2015-2020. Diagnosis of PD was performed based on the UK Parkinson's Disease Brain Bank criteria (Hughes et al., 1992). The presence of RBD in PD patients was evaluated by single-question screen for RBD (Postuma et al., 2012) and a semi-structured interview, whereas the diagnose of iRBD was done according to the criteria of the *International classification of sleep disorders – third edition* of the American Academy of Sleep Medicine published in 2014 (American Academy of Sleep Medicine, 2014). We included PD patients in early stages of disease (ePD; disease duration $\leq$ 4 years) and with age at clinical onset $\geq$ 45 years. Exclusion criteria were claustrophobia or any other contraindication to perform MRI at 7T, the presence of gene mutations associated with PD or potential causes of secondary parkinsonism and, for iRBD patients, the diagnosis of parkinsonism and/or dementia at the time of the MRI procedure, other sleep disorders or neurological conditions and current treatment with a drug known to induce RBD. According to these criteria, 54 ePD patients (aged 65 $\pm$ 8 [50–81] years old, 14 females / 40 males) and 36 patients with iRBD (aged 67 $\pm$ 10 [32-83] years old, 6 females / 30 males) were enrolled in this study, together with a population of 16 healthy controls (HC) (aged 59 $\pm$ 10 [43–77] years old, 7 females / 9 males) with no movement disorder and no neurological or psychiatric diseases, and comparable sex and age distribution. This study was approved by the local ethical committee and all participants gave their written informed consent.

2.2. Clinical data

Patients were clinically evaluated by neurologists experienced in movement disorders on the day of the MRI exam. For iRBD patients, age, sex and disease duration (i.e., the time elapsed since symptom onset as retrospectively evaluated by history) were recorded. For ePD patients, age, sex, disease duration, disease severity according with the Hoehn and Yahr (H&Y) score (Hoehn and Yahr, 1967), the presence of RBD, the Levodopa Equivalent Daily Dose (LEDD) and the clinical phenotype (i.e., Tremor Dominant -TD- or Postural Instability Gait Disorder -PIGD-) (Jankovic et al., 1990) were recorded. For all patients, motor function was assessed using the Unified Parkinson's Disease Rating Scale motor item (UPDRS-III) (Fahn et al., 1987), while cognitive screening was performed via Mini-Mental State Examination (MMSE) (Folstein et al., 1975).

After the MRI session, iRBD patients were clinically followed-up and both the follow-up duration (i.e., the time elapsed since symptom onset to the last follow-up available) and conversion time to synucleopathies, when applicable, were also recorded.

2.3. MRI acquisition hardware

All subjects underwent an ultra-high field MRI examination using a GE Healthcare Discovery MR950 7T MRI system (GE Healthcare, Milwaukee, WI, USA). The scanner was equipped with a two-channel transmitter/32-channel receiver head coil (Nova Medical, Wilmington, MA, USA) and a gradient system with maximum amplitude = 50 mT/m and slew rate = 200 T/m/s.

2.4. MRI imaging protocol

The MRI protocol included two 3D Gradient Recalled Multi-Echo sequences (Susceptibility Weighted Angiography – SWAN, GE Healthcare). One was acquired for the qualitative evaluation of the substantia nigra and had the following parameters: Repetition Time TR = 55.7 ms; eight equally spaced echoes with Echo Time TE_1: ΔTE : TE_8 = 5.57 : 5.1 : 41.5 ms; acquired voxel size = $0.5 \times 0.5 \times 1.2$ mm^3; reconstructed voxel size = $0.313 \times 0.313 \times 1.2$ mm^3; Flip Angle FA = 8°; in-plane FOV = 160×160 mm^2; through-plane coverage = 24 mm; parallel imaging ASSET (Array Coil Spatial Sensitivity Encoding) acceleration factor = 2, scan duration = 4'02". The acquisition targeted the midbrain and was oriented in the plane perpendicular to the floor of the fourth ventricle. This T2*-weighted sequence will be hereafter referred to as "morphological".

The second sequence was acquired to perform a quantitative assessment of iron deposition via QSM, and will be hereafter referred to as "complex-valued" dataset. The acquisition parameters were set as follows: TR = 54.1 ms; seven equally spaced echoes with TE_1: ΔTE : TE_7 = 5.6 : 6.0 : 41.8 ms; voxel size = $0.6 \times 0.6 \times 0.6$ mm^3; FA = 15°; in-plane FOV = 160×160 mm^2; through-plane coverage = 36 mm; parallel imaging ASSET (Array Coil Spatial Sensitivity Encoding) acceleration factor = 2, scan duration = 5'04". This sequence covered the brain from the ponto-mesencephalic junction to the splenium of the corpus callosum and was prescribed perpendicular to the floor of the fourth ventricle. Both the real and imaginary parts of the images obtained at each echo were saved and converted into magnitude and phase data.

2.5. QSM reconstruction pipeline and visual inspection

To obtain magnetic susceptibility maps, the processing of the "complex-valued" dataset was performed as follows. The raw phase images of individual echoes were unwrapped using a Laplacian-based algorithm (Li et al., 2012; Schofield and Zhu, 2003). A brain mask was generated using FSL 5.0.9 Brain Extraction Toolbox (*bet*) (Smith, 2002) (FMRIB Software Library, Oxford Centre for Functional MRI of the Brain, Oxford, UK) on the T2*-weighted image averaged across echoes and then used for the removal of the background field via V-SHARP (Schweser et al., 2011). QSM images were obtained by applying the iLSQR (Li et al., 2015, 2011) method separately to each echo, and then averaged to obtain one susceptibility map with higher signal-to-noise ratio (SNR) for statistical analyses (Denk and Rauscher, 2010). The Laplacian-based algorithm for phase unwrapping, V-SHARP and iLSQR are implemented in STI Suite (MATLAB toolbox, available at https://people.eecs.berkeley.edu/~chunlei.liu/software.html from UC Berkeley, Berkeley, CA, USA).

The TE-averaged magnitude images of the "complex-valued" datasets were evaluated by a neuroradiologist and graded based on the severity of motion artifacts into three categories: "none/mild" corresponding to non-visible or little motion artifact, "moderate" for detectable motion and "severe" for extreme motion artifacts. Images affected by "severe" motion artifacts were excluded from the analysis.

2.6. Qualitative evaluation of T2*-weighted "morphological" images

The "morphological" T2*-weighted images were averaged across TEs to increase SNR and CNR, by combining the contrast profiles of different echoes, in order to facilitate the delineation of a small structure such as N1. Then, they were visually inspected by two neuroradiologists experienced in neurodegenerative disorders and in ultra-high field MR imaging. The anatomy of the substantia nigra of each subject was examined according to established criteria (Cosottini et al., 2014), which assess the appearance of the trilaminar organization of the SN and the presence of an oval-shaped hyperintensity located dorsolaterally in the SN between two hypointense layers, corresponding to N1. In a consensus reading the images were labeled as "normal" when these structures were clearly visible in both left and right SN, or "pathological" when this was not the case in at least one side of the brainstem.

2.7. ROI creation

For the QSM-based quantitative analysis, we created an atlas of probabilistic regions of interests (ROIs) covering right and left N1. To this aim, we employed the following pipeline, also schematized in Fig. 1. First, the ROIs were manually segmented on the high-resolution TE-averaged T2*-weighted "morphological" images of healthy controls, on a single slice in which they were more clearly visible. Then, these images were employed to build a study-specific template (Fig. 1, step A) after bias-correction performed using *3dUnifize* in AFNI (Cox, 1996) and skull-stripping via *bet* in FSL 5.0.9. The template was created using *antsMultivariateTemplateConstruction* routine in ANTs (Advanced Normalization Tools) with Greedy-SyN approach and cross-correlation similarity metric (Avants et al., 2008). The ROIs of each healthy control were warped to the study-specific template by applying the corresponding transformation. As we are dealing with 2-D ROIs, we employed a linear interpolation method to avoid the loss of voxels belonging to the mask falling in between slices in the template space. Then, the obtained masks were binarized. Probabilistic ROIs were computed by averaging the transformed ROIs across all healthy controls and then thresholded to a probability of 0.4 (Fig. 1, step B).

2.8. Quantitative analysis

The TE-averaged magnitude image of the "complex-valued" dataset of each subject was bias-corrected, skull-stripped, and aligned to the corresponding "morphological" T2*-weighted image (Fig. 1, step C) by computing an affine transformation using *antsRegistration*. The bias-corrected skull-stripped "morphological" image of each patient was warped to the template space (Fig. 1, step D) via *antsRegistration* with Greedy-SyN approach and cross-correlation similarity metric (Avants et al., 2008). Then, these transformations were concatenated in order to warp the QSM image of each subject onto the template space.

For each subject, we identified the N1 (left or right) showing the highest mean susceptibility (χ) and considered it for statistical analysis, according to radiological criteria (Cosottini et al., 2014). Measured χ is reported in parts per million (ppm). To avoid assumptions on brain areas impaired by the disease, we did not reference QSM values with respect to any specific region (Acosta-Cabronero et al., 2016).

2.9. Statistical analysis

Statistical analysis was performed in MATLAB (MathWorks, Natick, MA, USA). Demographic and clinical data are expressed as mean ± standard deviation [range]. Sex distribution of the populations (PD, iRBD and HC) were compared using chi-square test. Age distributions and QSM data were analyzed via non-parametric statistical tests, i.e., Kruskal-Wallis omnibus tests followed by Dunn's test for post-hoc analysis and Dunn-Sidak correction for multiple comparisons. The area under the curve (AUC) of the receiver operating characteristic (ROC) curve was employed as a measure of diagnostic accuracy. The correlation between susceptibility values and disease duration was evaluated with the Spearman rank correlation test. The threshold of statistical significance was set to $p < 0.05$.

3. Results

The study-specific template and the probabilistic ROIs were computed from the "morphological" dataset of all HC. After visual inspection and rating of the magnitude image of the "complex-valued" dataset, 19 ePD patients, 6 patients with iRBD and 2 controls were excluded from QSM analysis due to severe motion artifacts. Then, the population used for QSM analysis included 14 HC, 30 iRBD patients and 35 ePD patients.
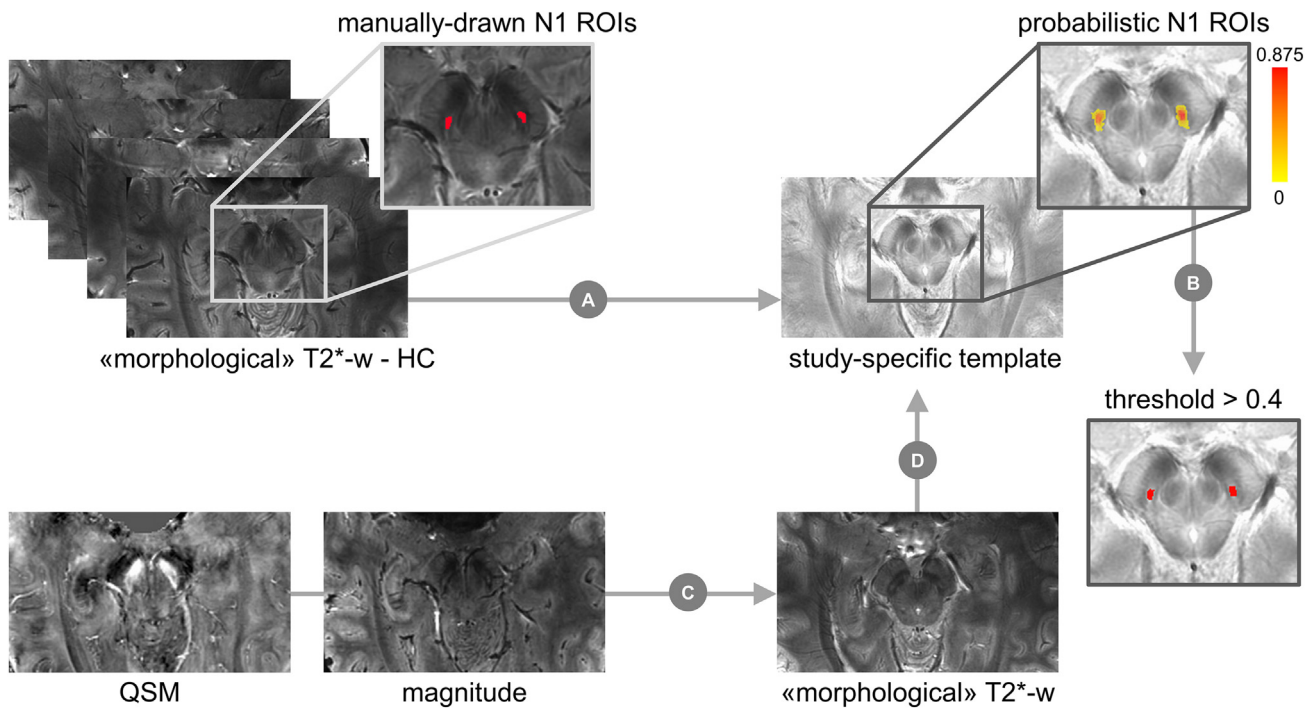
Fig. 1. Pipeline for template creation and QSM registration. ROIs encompassing N1 were manually drawn on the "morphological" T2*-weighted images of healthy controls. These images were bias-corrected, skull stripped and used to create a study-specific template (A). The probabilistic N1 ROIs were obtained by averaging the ROIs drawn on each control subject and warped to the template and were then threshold to 0.4 and binarized (B). The magnitude of the "complex-valued" dataset of each subject was aligned to the corresponding "morphological" T2*-weighted image (C). Then, a transformation warp was computed to transform the "morphological" image to the template space (D). Finally, the transformations were concatenated to warp the QSM image onto the template (C+D).

Table 1

Demographic and clinical information of the population used for QSM analysis. For the iRBD group, clinical scores reported here refers to the baseline evaluation at the time of the MRI session. The reported χ value refers to the nigrosome 1 with the highest QSM value for each subject (i.e., either left or right side). H&Y: Hoehn e Yahr; UPDRS-III; Unified Parkinson's Disease Rating Scale part III; MMSE: Mini Mental Status Examination; PIGD: Postural Instability and Gait Disorder; TD: Tremor Dominant; LEDD: Levodopa equivalent daily dose.

	PD	iRBD	HC
N	35	30	14
Sex (Females)	10	6	7
Age (years)	64 ± 8 [50-81]	66 ± 10 [32-81]	58 ± 10 [43-77]
Disease duration (years)	1.9 ± 0.9 [0.5-3]	5 ± 4 [1-13]	-
Follow-up duration (months)	-	24 ± 14 [5-50]	-
RBD symptoms	18	30	0
Phenotype	9 PIGD / 24 TD / 2 indeterminate	-	-
H&Y	1.6 ± 0.5 [1-2.5]	-	-
UPDRS-III	17.7 ± 6.1 [7-33]	2.6 ± 2.1 [0-7]	-
MMSE	29.5 ± 0.7 [27-30]	28.9 ± 2.0 [20-30]	-
Patients receiving treatment / LEDD [mg]	30 / 200 ± 125 [15-550]	-	-
N1 χ [ppm]	0.071 ± 0.025	0.044 ± 0.027	0.047 ± 0.015

The demographic and clinical information on the QSM population are summarized in Table 1.

We found no significant differences in sex distribution between groups. Age differences between groups were significant ($p < 0.01$): specifically, age distribution of the iRBD group was different from that of HC ($p < 0.01$). However, no significant correlation was found between age and χ values in N1 for any group.

Five iRBD patients (17%) developed PD (4 patients) or Dementia with Lewy Body (DLB) (1 patient) by the end of the follow-up observation period.

3.1. Qualitative imaging results

The appearance of N1 in the "morphological" T2*-weighted images was labeled as pathological in 29/35 (83%) ePD patients. In the iRBD group, one patient was excluded due to motion artifacts in the "morphological" image and 13/29 (45%) reported abnormal N1 appearance, including the 4 iRBD patients that converted to PD; the iRBD patient who converted to DLB had normal N1 appearance. In the control population, 2/14 (14%) exhibited N1 alterations. Normative and pathological imaging in exemplary subjects is displayed in Fig. 2.

3.2. Quantitative imaging results

After selecting the N1 ROI with the highest susceptibility for each subject, we compared the average QSM values between groups. Susceptibility values measured in iRBD patients who converted to synucleinopathies by the end of the follow-up period (iRBD-C) and in iRBD patients who had not yet converted (iRBD-NC) were not significantly different (Fig. 3A), therefore the two groups were considered together
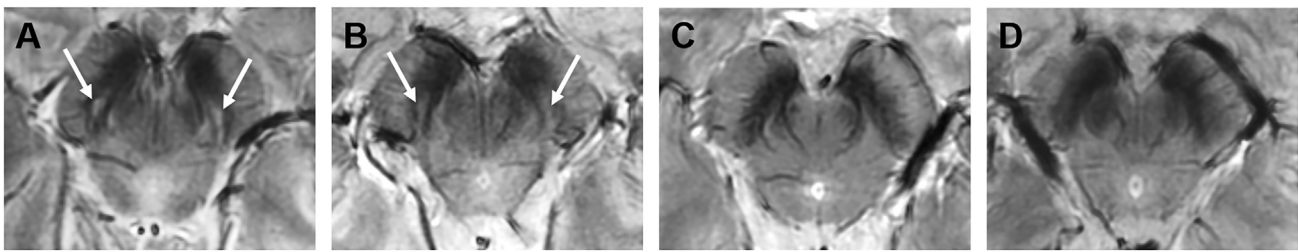
Fig. 2. "Morphological" T2*-weighted images of the nigrosome 1 in four representative subjects. In healthy controls (A), N1 appears as an oval-shaped hyperintensity (white arrows) surrounded by two hypointense layers and located dorsolaterally in the SN. This structure is also visible in some patients with iRBD (B), while this is not the case for other iRBD patients (C) and for most ePD patients (D).
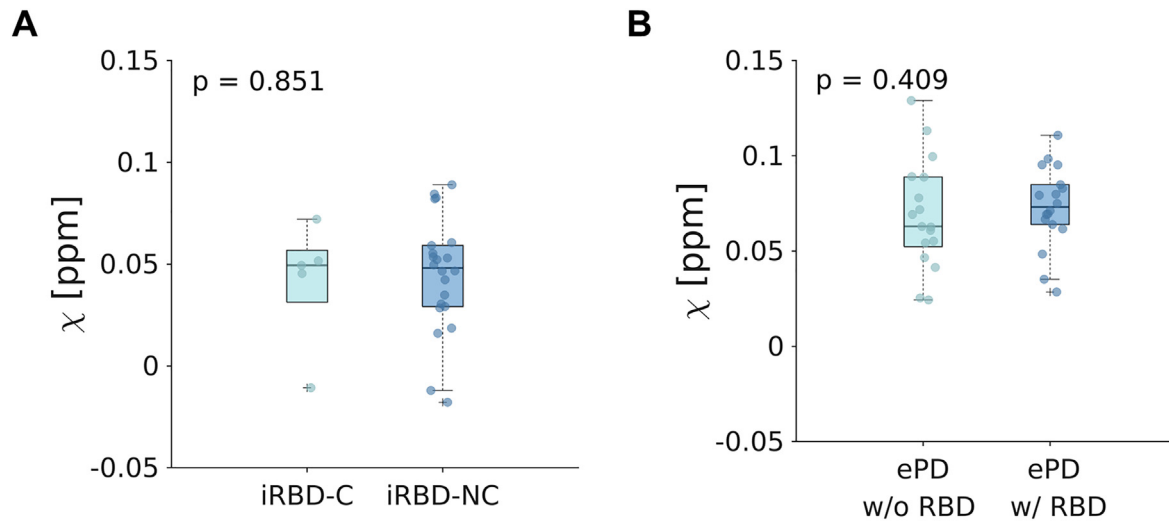

Fig. 3. Box plots showing comparisons of N1 susceptibility between groups: no significant differences were found between iRBD-C and iRBD-NC (panel A) and between ePD patients with or without RBD (panel B). The p-value of the Dunn's test is reported in the top-left corner of the corresponding plot.

for further analyses. Susceptibility in N1 was not significantly different in ePD patients with or without RBD symptoms (Fig. 3B).

The omnibus test revealed significant differences in N1 susceptibility between ePD, iRBD and HC ($p < 0.0001$): in particular, ePD patients showed increased χ with respect to both HC ($p < 0.01$) and iRBD ($p < 0.001$), as shown in Fig. 4A. The AUC obtained in discriminating ePD from iRBD patients was 0.76, with a specificity of 0.80 and a sensitivity of 0.74. Moreover, ePD and HC could be discriminated with an AUC of 0.81, a specificity of 0.86 and a sensitivity of 0.74 (Fig. 4B).

The iRBD population was then split into two subgroups: one including patients with normal N1 appearance in the T2*-weighted image (iRBD-) and one comprising those with pathological imaging (iRBD+). Although χ difference did not reach statistical significance, we measured higher QSM values in iRBD+ patients (Fig. 5A). This led to a non-significant difference with the ePD group (Fig. 5B), in contrast to what reported when considering the entire iRBD cohort (Fig. 4A). However, no statistically significant difference is reported comparing iRBD+ to HC.

Statistically significant positive correlation ($r = 0.475$; $p < 0.01$) emerged between susceptibility in N1 and disease duration in iRBD patients (Fig. 6A). Instead, no significant correlation was found between N1 χ and disease duration in ePD patients (Fig. 6B).

4. Discussion

This study focused on exploring the potential of N1 magnetic susceptibility as a non-invasive biomarker for synucleinopathies and their prodromal stages, such as iRBD. Specifically, we recruited ePD patients, iRBD patients and healthy controls and acquired GRE sequences for vi-

sual inspection and susceptibility mapping of the SN on a 7T MRI system. We measured susceptibility in order to detect group differences in iron load and assess its increase as long as the disease progresses. To the best of our knowledge, this is the first QSM study targeting N1 in a population of iRBD patients at 7T.

Iron concentration in N1 was higher for ePD patients than for the control group and most ePD patients had N1 hypointensity. This is in agreement with previous studies that investigated susceptibility in SNc (Barbosa et al., 2015; Chen et al., 2019; Du et al., 2018, 2016; Takahashi et al., 2018b; Xuan et al., 2017) and in its dorsolateral portion (Takahashi et al., 2018a), and the radiological appearance of SN (Blazejewska et al., 2013; Cosottini et al., 2015, 2014; Kim et al., 2016; Schmidt et al., 2017).

In PD patients, iron accumulation in SN is a well-documented finding. Even though the temporal relationship between iron storage and the death of neuromelanin containing dopaminergic cells has not been completely elucidated, the role of iron in the pathogenesis of PD is well supported (Sian-Hülsmann et al., 2011). A number of mechanisms of iron-related damage of dopaminergic cells have been suggested, probably interplaying among each other, and the microglial activation may exacerbate the process (Sian-Hülsmann et al., 2011). The increase of iron in SN has been found in many different cell types including inflammatory cells and melanized dopamine neurons of SNc (Jellinger et al., 1990; Youdim and Riederer, 1993). In particular, numerous ferritin-positive reactive microglia cells have been found in the area of degenerating neurons (Jellinger et al., 1990), and this might be at least in part the source of the susceptibility effect detected with MRI.

The spatial distribution of iron storage within SN matches with that of dopaminergic neuron loss, further suggesting a relationship between
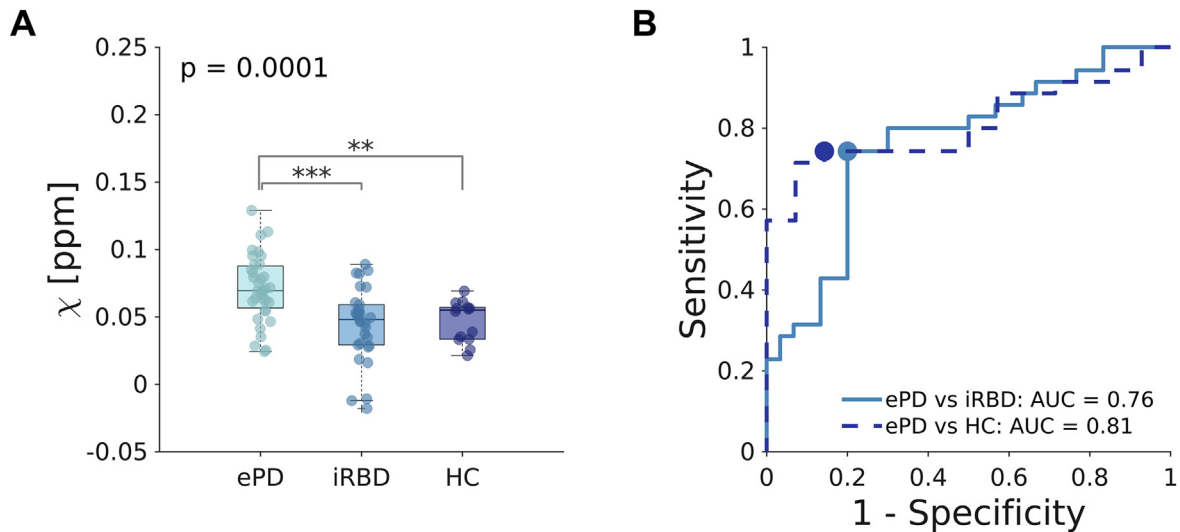
Fig. 4. Box plot displaying group differences in N1 susceptibility between ePD patients, iRBD patients and HC (panel A). In the top left corner, we reported the p-value of the omnibus Kruskal-Wallis test. Post-hoc Dunn's tests reaching significance after Dunn-Sidak correction are indicated by asterisks (* $p < 0.05$, ** $p < 0.01$, *** $p < 0.001$). Panel B shows the ROC curves computed when discriminating ePD from iRBD (solid line) and ePD from HC (dashed line). The dots represent the optimal cut-off values of each curve.
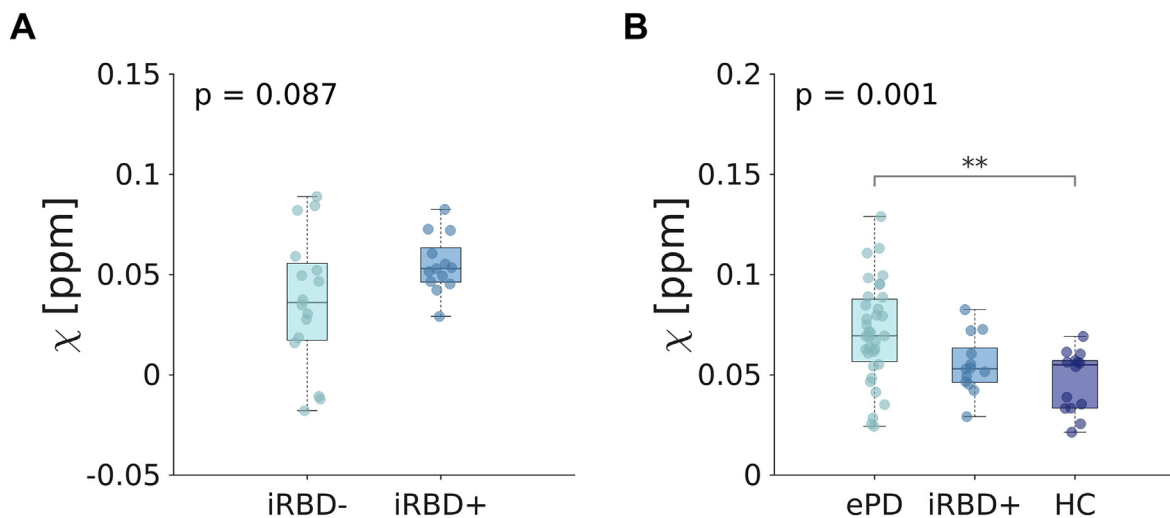

Fig. 5. Box plot displaying group differences in N1 susceptibility considering iRBD patients with normal (iRBD-) and pathological (iRBD+) qualitative imaging separately. Although the difference does not reach significance, iRBD+ patients reported slightly higher χ, on average, than those in iRBD- group (panel A). Similarly, panel B shows that the difference in N1 χ with ePD patients is not significant when considering iRBD+ patients only instead of the whole iRBD population (Fig. 4A). In the top left corner, we reported the p-value of the omnibus Kruskal-Wallis test. Post-hoc Dunn's tests reaching significance after Dunn-Sidak correction are indicated by the asterisks (* $p < 0.05$, ** $p < 0.01$).

the two processes. Indeed, increased iron levels have been found in post-mortem samples of SNc but not in SN pars reticulata (Jellinger et al., 1990; Sofic et al., 1991), and the ventrolateral tier of the SNc, which corresponds to N1, is the first region affected by neuronal loss and the most affected throughout the disease (Damier et al., 1999; Fearnley and Lees, 1991). N1 is, therefore, the best target within the SN for an early detection of the pathology.

The accumulation of iron in N1 in the iRBD group is comparable to that in HC, in accordance with previous studies that observed no differences in T2* in SN between iRBD patients and controls (Lee et al., 2014; Pyatigorskaya et al., 2017) and with recent works that considered average QSM values in the whole SN (Chen et al., 2021; Zhang et al., 2021) or in its functional subregions (Biondetti et al., 2021). However, another study reported higher susceptibility in iRBD patients compared to HC, but significantly lower than in PD (Sun et al., 2020). Besides,

also the number of iRBD patients with N1 hypointensity noted in our study is in line with the wide range of positive cases described in the literature (Bae et al., 2018; Barber et al., 2020; De Marzi et al., 2016; Frosini et al., 2017; Zhang et al., 2021). The slightly inconsistent results reported so far can be accounted for by the different degree of striatal dopamine deficiency in iRBD patients enrolled in each study, and by the use of a reference region for susceptibility measures.

The variability of the quantitative and qualitative changes within SN of iRBD patients could be related to the proximity to the conversion. iRBD+ patients have a peculiar level of putaminal dopaminergic SPECT activity as it has been found lower than in both iRBD- patients (Barber et al., 2020) and healthy controls (Bae et al., 2018), but higher than in PD patients (Bae et al., 2018). Moreover, iRBD patients with dopaminergic dysfunction have an increased risk of short-term conversion (Arnaldi et al., 2021; Iranzo et al., 2010). Taken together, these
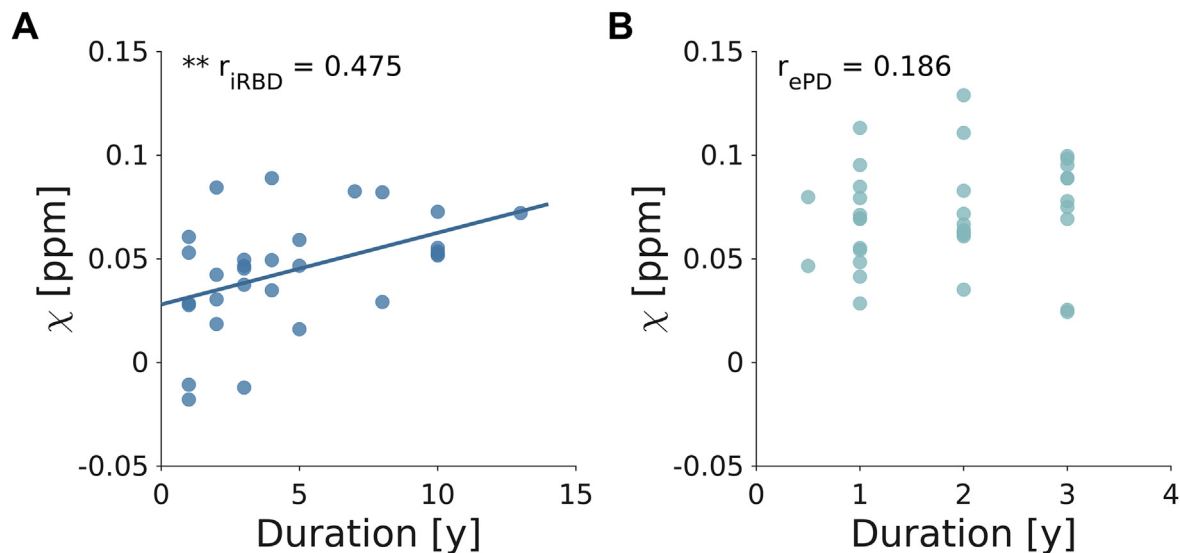
Fig. 6. Correlation of N1 χ and disease duration. A significant positive correlation was found for iRBD (** $p < 0.01$; panel A) but not for the ePD group (panel B).

data suggest that iron may accumulate in SN later during the disease process and iRBD- patients might have been imaged when the abnormal iron accumulation had not yet occurred or had not yet enough to be detected with MRI. Therefore, the number of patients with impaired putaminal dopaminergic projections and the degree of the dopaminergic deficiency could affect the results of both qualitative and quantitative MR studies. This is also testified by the variable prevalence of pathological MR imaging reported in iRBD patients, ranging between 27.5% and 77% (Bae et al., 2018; Barber et al., 2020; De Marzi et al., 2016; Frosini et al., 2017) and the lack of significant differences between susceptibility values measured in ePD and iRBD+ patients.

Methodological differences might influence the variable incidence of SN changes in iRBD. In our analysis and in two other studies (Chen et al., 2021; Zhang et al., 2021) susceptibility values were not referenced to a specific anatomical area, because the populations considered in this study may show a diffuse pattern of pathological alterations in both gray and white matter: this strategy may lead to slightly different results from those obtained with referencing (Biondetti et al., 2021; Sun et al., 2020). In addition, we selected a small ROI covering only the nigrosome 1 while in other studies the whole SN was explored (Chen et al., 2021; Sun et al., 2020; Zhang et al., 2021). Further investigations are required to settle this discrepancy.

The correlation between N1 χ and duration of iRBD points out that iron accumulation increases along with the disease evolution, confirming a previous observation (Sun et al., 2020). As no differences are reported between ePD patients with or without RBD, we suppose that the gradual increment in iron stores in N1 may happen prior to the emergence of motor symptoms, irrespective of the presence of RBD. To confirm this hypothesis, longitudinal studies in the general population and in patients at risk of developing synucleinopathies are needed. Moreover, we did not find any correlation between ePD duration and susceptibility in N1, so it can be assumed that further iron accumulation is not significant once motor symptoms appear. Concerning this finding, the literature provides inconsistent observations, as the positive correlation of susceptibility in SN with disease duration was reported by some previous works (He et al., 2015), especially for PD patients with longer disease duration (Du et al., 2016) but not confirmed by others (Sun et al., 2020). In this regard, one possible confounding factor relates to the prevalence of PD patients with short disease duration generally enrolled in these studies. In our work, PD patients had a disease duration shorter than 4 years and potential long-term correlations would remain undetected. Another possible explanation is the different percentage of

dopaminergic neurons which die after clinical onset in the whole SNc (where about 52% of cells are still alive) and in its ventrolateral tier (where there is only about 32% of cells left) (Fearnley and Lees, 1991). Even though the neuronal death continues exponentially, the influence on susceptibility measures is expected to be greater for SNc than for N1. On these premises, we may hypothesize that the iron load in N1 is not an index of disease progression, at least in the first years of PD, but rather a marker of ongoing neurodegeneration in presymptomatic stages. It is still unknown whether the trajectory of N1 iron accumulation is different in iRBD patients who will convert to PD compared to those who will progress to MSA or DLB. Longitudinal assessment of iRBD patients is necessary to confirm N1 iron load as a marker of disease progression and to investigate patterns of N1 χ in the prodromal stages of each synucleinopathy.

The absence of a correlation between N1 χ and age in ePD patients, iRBD and control subjects is in line with the age-related iron levels in the SN, which are not expected to increase after the fourth decade (Zecca et al., 2001), and with the limited age-related neuronal loss in the ventrolateral tier of SNc (Fearnley and Lees, 1991). For this reason, we would not expect the age difference between iRBD patients and HC to significantly affect the results of this study.

From the methodological point of view, the ROIs covering N1 used in this study were manually drawn by an experienced neuroradiologist on a high-resolution T2*-weighted image of the control subjects. Then, a probabilistic atlas was created and used to evaluate N1 χ in all subjects. The rationale for this approach concerned the absence of a published N1 ROI and the critical issues in drawing it on structures with pathological appearance. This semi-automated approach removed the user's discretionality in drawing the small N1 ROIs on the single patient. The probability threshold value of 0.4 was empirically chosen by a neuroradiologist as the optimal tradeoff between the inclusion of most N1 voxels and the exclusion of the neighboring tissues. To ensure that the results were not affected by registration errors, a neuroradiologist checked the alignment of each subject to the template. The N1 probabilistic ROI created in this work can be applied to future studies and translated to clinical field strength, provided that high spatial resolution is achieved. This constraint is due to the small dimension of N1 and represents the rationale for performing this study on an ultra-high field MR system.

An alternative approach for future studies may involve the usage of histogram and pattern analysis on the whole volume of SN. This would allow the exploration of the tails of the χ distribution and of its fine

spatial variations (Lancione et al., 2022; Zhang et al., 2020), so as to also take into account N1 spatial variants (Cheng et al., 2020).

The choice of selecting and analyzing the N1 with the highest susceptibility is supported by clinical and radiological findings and aimed to maximize the sensitivity in revealing neurodegeneration in both ePD and iRBD patients. Motor symptoms of PD are, indeed, usually asymmetric (Balestrino and Schapira, 2020) and this asymmetry matches with the different N1 visibility (Noh et al., 2015). It is therefore commonly accepted to define an imaging "pathological" in case of the loss of N1 hyperintensity in at least one side of the midbrain (Blazejewska et al., 2013; Cosottini et al., 2014).

In conclusion, we reported that the iron content in N1 of iRBD patients is comparable to those in HC but it grows as the disease evolves. On the contrary, ePD patients showed increased N1 iron load with respect to iRBD and HC but our results suggest that it remains roughly unaltered during disease evolution. Even though N1 iron content may not be an index of PD progression, at least during its first stages, our work suggests the potential of N1 iron load detection via QSM as a presymptomatic biomarker for the assessment of PD and of ongoing neurodegeneration in its prodromal stages, such as iRBD. If this finding is confirmed, the estimation of N1 iron may be used in clinical trials as a surrogate marker to monitor the effectiveness of neuroprotective drugs. Longitudinal studies are warranted to get further insights into the mechanisms of iron accumulation and their causal relationship to disease development.

Data and code availability statement

Data and code may be provided to interested researchers upon request to the corresponding author, after clearance from the IRB.

Declaration of Competing Interest

Mirco Cosottini received a speaker honorarium from GE Healthcare. All other authors declare no conflict of interest.

Credit authorship contribution statement

Marta Lancione: Conceptualization, Methodology, Software, Formal analysis, Investigation, Visualization, Writing – original draft, Writing – review & editing. **Graziella Donatelli:** Conceptualization, Methodology, Formal analysis, Investigation, Visualization, Writing – original draft, Writing – review & editing. **Eleonora Del Prete:** Methodology, Investigation, Resources, Writing – review & editing. **Nicole Campese:** Methodology, Investigation, Resources, Writing – review & editing. **Daniela Frosini:** Conceptualization, Methodology, Investigation, Resources, Writing – review & editing. **Matteo Cencini:** Methodology, Formal analysis, Visualization, Writing – review & editing. **Mauro Costagli:** Methodology, Software, Investigation, Writing – review & editing. **Laura Biagi:** Methodology, Investigation, Writing – review & editing. **Giacomo Lucchi:** Methodology, Formal analysis, Writing – review & editing. **Michela Tosetti:** Resources, Writing – review & editing. **Massimiliano Godani:** Resources, Writing – review & editing. **Dario Arnaldi:** Resources, Writing – review & editing. **Michele Terzaghi:** Resources, Writing – review & editing. **Federica Provini:** Resources, Writing – review & editing. **Claudio Pacchetti:** Resources, Writing – review & editing. **Pietro Cortelli:** Resources, Writing – review & editing. **Enrica Bonanni:** Resources, Investigation, Writing – review & editing. **Roberto Ceravolo:** Conceptualization, Resources, Investigation, Project administration, Funding acquisition, Writing – review & editing. **Mirco Cosottini:** Conceptualization, Resources, Investigation, Project administration, Funding acquisition, Writing – review & editing.

Funding

References

Acosta-Cabronero, J., Betts, M.J., Cardenas-Blanco, A., Yang, S., Nestor, P.J., 2016. *In vivo* MRI mapping of brain iron deposition across the adult lifespan. Neurobiol. Dis. 36, 364–374. doi:10.1523/JNEUROSCI.1907-15.2016.

American Academy of Sleep Medicine, 2014. International classification of sleep disorders, third ed. American Academy of Sleep Medicine, Darien, IL.

An, H., Zeng, X., Niu, T., Li, G., Yang, J., Zheng, L., Zhou, W., Liu, H., Zhang, M., Huang, D., Li, J., 2018. Quantifying iron deposition within the substantia nigra of Parkinson's disease by quantitative susceptibility mapping. J. Neurol. Sci. 386, 46–52. doi:10.1016/j.jns.2018.01.008.

Arnaldi, D., Chincarini, A., Hu, M.T., Sonka, K., Boeve, B., Miyamoto, T., Puligheddu, M., De Cock, V.C., Terzaghi, M., Plazzi, G., Tachibana, N., Morbelli, S., Rolinski, M., Dusek, P., Lowe, V., Miyamoto, M., Figorilli, M., Verbizier, D.De, Bossert, I., Antelmi, E., Meli, R., Barber, T.R., Trnka, J., Miyagawa, T., Serra, A., Pizza, F., Bauckneht, M., Bradley, K.M., Zogala, D., McGowan, D.R., Jordan, L., Manni, R., Nobili, F., 2021. Dopaminergic imaging and clinical predictors for phenoconversion of REM sleep behaviour disorder. Brain 144, 278–287. doi:10.1093/BRAIN/AWAA365.

Avants, B.B., Epstein, C.L., Grossman, M., Gee, J.C., 2008. Symmetric diffeomorphic image registration with cross-correlation: Evaluating automated labeling of elderly and neurodegenerative brain. Med. Image Anal. 12, 26–41. doi:10.1016/j.media.2007.06.004.

Bae, Y.J., Kim, J.M., Kim, K.J., Kim, E., Park, H.S., Kang, S.Y., Yoon, I.Y., Lee, J.Y., Jeon, B., Kim, S.E., 2018. Loss of substantia nigra hyperintensity at 3.0-T MR imaging in idiopathic REM sleep behavior disorder: comparison with 123I-FP-CIT SPECT. Radiology 287, 285–293. doi:10.1148/radiol.2017162486.

Balestrino, R., Schapira, A.H.V., 2020. Parkinson disease. Eur. J. Neurol. doi:10.1111/ene.14108.

Barber, T.R., Griffanti, L., Bradley, K.M., McGowan, D.R., Lo, C., Mackay, C.E., Hu, M.T., Klein, J.C., 2020. Nigrosome 1 imaging in REM sleep behavior disorder and its association with dopaminergic decline. Ann. Clin. Transl. Neurol. 7, 26–35. doi:10.1002/acn3.50962.

Barbosa, J.H.O., Santos, A.C., Tumas, V., Liu, M., Zheng, W., Haacke, E.M., Salmon, C.E.G., 2015. Quantifying brain iron deposition in patients with Parkinson's disease using quantitative susceptibility mapping, R2 and R2. Magn. Reson. Imaging 33, 559–565. doi:10.1016/j.mri.2015.02.021.

Biondetti, E., Santin, M.D., Valabrègue, R., Mangone, G., Gaurav, R., Pyatigorskaya, N., Hutchison, M., Yahia-Cherif, L., Villain, N., Habert, M.-O., Arnulf, I., Leu-Semenescu, S., Dodet, P., Vila, M., Corvol, J.-C., Vidailhet, M., Lehéricy, S., 2021. The spatiotemporal changes in dopamine, neuromelanin and iron characterizing Parkinson's disease. Brain 144. doi:10.1093/brain/awab191.

Blazejewska, A.I., Schwarz, S.T., Pitiot, A., Stephenson, M.C., Lowe, J., Bajaj, N., Bowtell, R.W., Auer, D.P., Gowland, P.A., 2013. Visualization of nigrosome 1 and its loss in PD: pathoanatomical correlation and *in vivo* 7 T MRI. Neurology 81, 534–540. doi:10.1212/WNL.0b013e31829e6fd2.

Chen, Q., Boeve, B.F., Forghanian-Arani, A., Senjem, M.L., Jack, C.R., Przybelski, S.A., Lesnick, T.G., Kremers, W.K., Fields, J.A., Schwarz, C.G., Gunter, J.L., Trzasko, J.D., Graff-Radford, J., Savica, R., Knopman, D.S., Dickson, D.W., Ferman, T.J., Graff-Radford, N., Petersen, R.C., Kantarci, K., 2021. MRI quantitative susceptibility mapping of the substantia nigra as an early biomarker for Lewy body disease. J. Neuroimaging JON 12878. doi:10.1111/jon.12878.

Chen, Q., Chen, Y., Zhang, Y., Wang, F., Yu, H., Zhang, C., Jiang, Z., Luo, W., 2019. Iron deposition in Parkinson's disease by quantitative susceptibility mapping. BMC Neurosci. 20, 23. doi:10.1186/s12868-019-0505-9.

Cheng, Z., He, N., Huang, P., Li, Y., Tang, R., Sethi, S.K., Ghassaban, K., Yerramsetty, K.K., Palutla, V.K., Chen, S., Yan, F., Haacke, E.M., 2020. Imaging the nigrosome 1 in the substantia nigra using susceptibility weighted imaging and quantitative susceptibility mapping: an application to Parkinson's disease. NeuroImage Clin. 25, 102103. doi:10.1016/j.nicl.2019.102103.

Cicero, C.E., Giuliano, L., Luna, J., Zappia, M., Preux, P.M., Nicoletti, A., 2021. Prevalence of idiopathic REM behavior disorder: a systematic review and meta-analysis. Sleep 44, 1–10. doi:10.1093/SLEEP/ZSAA294.

Cosottini, M., Frosini, D., Pesaresi, I., Costagli, M., Biagi, L., Ceravolo, R., Bonuccelli, U., Tosetti, M., 2014. MR imaging of the substantia nigra at 7 T enables diagnosis of Parkinson disease. Radiology 271, 831–838. doi:10.1148/radiol.14131448.

Cosottini, M., Frosini, D., Pesaresi, I., Donatelli, G., Cecchi, P., Costagli, M., Biagi, L., Ceravolo, R., Bonuccelli, U., Tosetti, M., 2015. Comparison of 3T and 7T susceptibility-weighted angiography of the substantia nigra in diagnosing Parkinson disease. Am. J. Neuroradiol. 36, 461–466. doi:10.3174/ajnr.A4158.

Costagli, M., Donatelli, G., Biagi, L., Caldarazzo Ienco, E., Siciliano, G., Tosetti, M., Cosottini, M., 2016. Magnetic susceptibility in the deep layers of the primary motor cortex in amyotrophic lateral sclerosis. NeuroImage Clin. 12, 965–969. doi:10.1016/j.nicl.2016.04.011.

Cox, R.W., 1996. AFNI: software for analysis and visualization of functional magnetic resonance neuroimages. Comput. Biomed. Res. 29, 162–173. doi:10.1006/CBMR.1996.0014.

Damier, P., Hirsch, E.C., Agid, Y., Graybiel, A.M., 1999. The substantia nigra of the human brainII. Patterns of loss of dopamine-containing neurons in Parkinson's disease. Brain 122, 1437–1448. doi:10.1093/BRAIN/122.8.1437.

De Marzi, R., Seppi, K., Högl, B., Müller, C., Scherfler, C., Stefani, A., Iranzo, A., Tolosa, E., Santamarìa, J., Gizewski, E., Schocke, M., Skalla, E., Kremser, C., Poewe, W., 2016. Loss of dorsolateral nigral hyperintensity on 3.0 tesla susceptibility-weighted imaging in idiopathic rapid eye movement sleep behavior disorder. Ann. Neurol. 79, 1026–1030. doi:10.1002/ana.24646.

Denk, C., Rauscher, A., 2010. Susceptibility weighted imaging with multiple echoes. J. Magn. Reson. Imaging 31, 185–191. doi:10.1002/jmri.21995.

Du, G., Lewis, M.M., Sica, C., He, L., Connor, J.R., Kong, L., Mailman, R.B., Huang, X., 2018. Distinct progression pattern of susceptibility in the substantia nigra of Parkinson's patients. Mov. Disord. 33, 1423–1431. doi:10.1002/mds.27318.

Du, G., Liu, T., Lewis, M.M., Kong, L., Wang, Y., Connor, J., Mailman, R.B., Huang, X., 2016. Quantitative susceptibility mapping of the midbrain in Parkinson's disease. Mov. Disord. 31, 317–324. doi:10.1002/mds.26417.

Fahn, S., Elton, R.L., Fahn, S., Marsden, C., Calne, D., Goldstein, M.Members of the UP-DRS Development Committee, 1987. Unified Parkinson's disease rating scale. Recent Development in Parkinson's Disease. Macmillan.

Fearnley, J.M., Lees, A.J., 1991. Ageing and parkinson's disease: substantia nigra regional selectivity. Brain 114, 2283–2301. doi:10.1093/brain/114.5.2283.

Folstein, M.F., Folstein, S.E., McHugh, P.R., 1975. Mini-mental state". A practical method for grading the cognitive state of patients for the clinician. J. Psychiatr. Res. 12, 189–198. doi:10.1016/0022-3956(75)90026-6.

Frosini, D., Cosottini, M., Donatelli, G., Costagli, M., Biagi, L., Pacchetti, C., Terzaghi, M., Cortelli, P., Arnaldi, D., Bonanni, E., Tosetti, M., Bonuccelli, U., Ceravolo, R., 2017. Seven tesla MRI of the substantia nigra in patients with rapid eye movement sleep behaviour disorder. Park. Relat. Disord. 43, 105–109. doi:10.1016/j.parkreldis.2017.08.002.

Galbiati, A., Verga, L., Giora, E., Zucconi, M., Ferini-Strambi, L., 2019. The risk of neurodegeneration in REM sleep behavior disorder: a systematic review and meta-analysis of longitudinal studies. Sleep Med. Rev. doi:10.1016/j.smrv.2018.09.008.

Gibb, W.R.G., Lees, A.J., 1988. The relevance of the Lewy body to the pathogenesis of idiopathic Parkinson's disease. J. Neurol. Neurosurg. Psychiatry doi:10.1136/jnnp.51.6.745.

He, N., Ling, H., Ding, B., Huang, J., Zhang, Y., Zhang, Z., Liu, C., Chen, K., Yan, F., 2015. Region-specific disturbed iron distribution in early idiopathic Parkinson's disease measured by quantitative susceptibility mapping. Hum. Brain Mapp. 36, 4407–4420. doi:10.1002/hbm.22928.

Hoehn, M.M., Yahr, M.D., 1967. Parkinsonism: onset, progression, and mortality. Neurology 17, 427–442. doi:10.1212/wnl.17.5.427.

Hughes, A.J., Daniel, S.E., Kilford, L., Lees, A.J., 1992. Accuracy of clinical diagnosis of idiopathic Parkinson's disease: a clinico-pathological study of 100 cases. J. Neurol. Neurosurg. Psychiatry 55 (3), 181–184. doi:10.1136/jnnp.55.3.181.

Iranzo, A., Lomeña, F., Stockner, H., Valldeoriola, F., Vilaseca, I., Salamero, M., Molinuevo, J.L., Serradell, M., Duch, J., Pavía, J., Gallego, J., Seppi, K., Högl, B., Tolosa, E., Poewe, W., Santamaria, J., 2010. Decreased striatal dopamine transporter uptake and substantia nigra hyperechogenicity as risk markers of synucleinopathy in patients with idiopathic rapid-eye-movement sleep behaviour disorder: a prospective study. Lancet Neurol. 9, 1070–1077. doi:10.1016/S1474-4422(10)70216-7.

Iranzo, A., Santamaría, J., Valldeoriola, F., Serradell, M., Salamero, M., Gaig, C., Niñerola-Baizán, A., Sánchez-Valle, R., Lladó, A., De Marzi, R., Stefani, A., Seppi, K., Pavia, J., Högl, B., Poewe, W., Tolosa, E., Lomeña, F., 2017. Dopamine transporter imaging deficit predicts early transition to synucleinopathy in idiopathic rapid eye movement sleep behaviour disorder. Ann. Neurol. 82, 419–428. doi:10.1002/ANA.25026.

Jankovic, J., McDermott, M., Carter, J., Gauthier, S., Goetz, C., Golbe, L., Huber, S., Koller, W., Olanow, C., Shoulson, I., Stern, M., Tanner, C., Weiner, W., 1990. Variable expression of Parkinson's disease. Neurology 40, 1529. doi:10.1212/WNL.40.10.1529.

Jellinger, K., Paulus, W., Grundke-Iqbal, I., Riederer, P., Youdim, M.B.H., 1990. Brain iron and ferritin in Parkinson's and Alzheimer's diseases. J. Neural Transm. Park. Dis. Dement. Sect. 2, 327–340. doi:10.1007/BF02252926.

Kim, J.M., Jeong, H.J., Bae, Y.J., Park, S.Y., Kim, E., Kang, S.Y., Oh, E.S., Kim, K.J., Jeon, B., Kim, S.E., Cho, Z.H., Kim, Y.B., 2016. Loss of substantia nigra hyperintensity on 7 Tesla MRI of Parkinson's disease, multiple system atrophy, and progressive supranuclear palsy. Parkinsonism Relat. Disord. 26, 47–54. doi:10.1016/J.PARKRELDIS.2016.01.023.

Lancione, M., Cencini, M., Costagli, M., Donatelli, G., Tosetti, M., Giannini, G., Zangaglia, R., Calandra-Buonaura, G., Pacchetti, C., Cortelli, P., Cosottini, M., 2022. Diagnostic accuracy of quantitative susceptibility mapping in multiple system atrophy: the impact of echo time and the potential of histogram analysis. NeuroImage Clin. 34, 102989. doi:10.1016/J.NICL.2022.102989.

Langkammer, C., Pirpamer, L., Seiler, S., Deistung, A., Schweser, F., Franthal, S., Homayoon, N., Katschnig-Winter, P., Koegl-Wallner, M., Pendl, T., Stoegerer, E.M., Wenzel, K., Fazekas, F., Ropele, S., Reichenbach, J.R., Schmidt, R., Schwingenschuh, P., 2016. Quantitative susceptibility mapping in parkinson's disease. PLoS One 11, e0162460. doi:10.1371/journal.pone.0162460.

Langkammer, C., Schweser, F., Krebs, N., Deistung, A., Goessler, W., Scheurer, E., Sommer, K., Reishofer, G., Yen, K., Fazekas, F., Ropele, S., Reichenbach, J.R., 2012. Quantitative susceptibility mapping (QSM) as a means to measure brain iron? A post mortem validation study. Neuroimage 62, 1593–1599. doi:10.1016/J.NEUROIMAGE.2012.05.049.

Lee, J.H., Han, Y.H., Cho, J.W., Lee, J.S., Lee, S.J., Kim, D.J., Kim, T.H., Kang, B.M., Kim, T.H., Mun, C.W., 2014. Evaluation of brain iron content in idiopathic REM sleep behavior disorder using quantitative magnetic resonance imaging. Park. Relat. Disord. 20, 776–778. doi:10.1016/j.parkreldis.2014.03.023.

Li, W., Wang, N., Yu, F., Han, H., Cao, W., Romero, R., Tantiwongkosi, B., Duong, T.Q., Liu, C., 2015. A method for estimating and removing streaking artifacts in quantitative susceptibility mapping. Neuroimage 108, 111–122. doi:10.1016/j.neuroimage.2014.12.043.

Li, W., Wu, B., Avram, A.V., Liu, C., 2012. Magnetic susceptibility anisotropy of human brain in vivo and its molecular underpinnings. Neuroimage 59, 2088–2097. doi:10.1016/j.neuroimage.2011.10.038.

Li, W., Wu, B., Liu, C., 2011. Quantitative susceptibility mapping of human brain reflects spatial variation in tissue composition. Neuroimage 55, 1645–1656. doi:10.1016/j.neuroimage.2010.11.088.

Murakami, Y., Kakeda, S., Watanabe, K., Ueda, I., Ogasawara, A., Moriya, J., Ide, S., Futatsuya, K., Sato, T., Okada, K., Uozumi, T., Tsuji, S., Liu, T., Wang, Y., Korogi, Y., 2015. Usefulness of quantitative susceptibility mapping for the diagnosis of Parkinson disease. Am. J. Neuroradiol. 36, 1102–1108. doi:10.3174/ajnr.A4260.

Noh, Y., Sung, Y.H., Lee, J., Kim, E.Y., 2015. Nigrosome 1 detection at 3T MRI for the diagnosis of early-stage idiopathic Parkinson disease: assessment of diagnostic accuracy and agreement on imaging asymmetry and clinical laterality. Am. J. Neuroradiol. 36, 2010–2016. doi:10.3174/ajnr.A4412.

Postuma, R.B., Arnulf, I., Hogl, B., Iranzo, A., Miyamoto, T., Dauvilliers, Y., Oertel, W., Ju, Y.El, Puligheddu, M., Jennum, P., Pelletier, A., Wolfson, C., Leu-Semenescu, S., Frauscher, B., Miyamoto, M., Cochen De Cock, V., Unger, M.M., Stiasny-Kolster, K., Livia Fantini, M., Montplaisir, J.Y., 2012. A single-question screen for rapid eye movement sleep behavior disorder: a multicenter validation study. Mov. Disord. 27, 913–916. doi:10.1002/MDS.25037.

Postuma, R.B., Berg, D., Stern, M., Poewe, W., Olanow, C.W., Oertel, W., Obeso, J., Marek, K., Litvan, I., Lang, A.E., Halliday, G., Goetz, C.G., Gasser, T., Dubois, B., Chan, P., Bloem, B.R., Adler, C.H., Deuschl, G., 2015a. MDS clinical diagnostic criteria for Parkinson's disease. Mov. Disord. 30, 1591–1601. doi:10.1002/MDS.26424.

Postuma, R.B., Gagnon, J.F., Bertrand, J.A., Génier Marchand, D., Montplaisir, J.Y., 2015b. Parkinson risk in idiopathic REM sleep behavior disorder: preparing for neuroprotective trials. Neurology 84, 1104–1113. doi:10.1212/WNL.0000000000001364.

Pyatigorskaya, N., Gaurav, R., Arnaldi, D., Leu-Semenescu, S., Yahia-Cherif, L., Valabregue, R., Vidailhet, M., Arnulf, I., Lehericy, S., 2017. Magnetic resonance imaging biomarkers to assess substantia nigra damage in idiopathic rapid eye movement sleep behavior disorder. Sleep 40. doi:10.1093/sleep/zsx149.

Schenck, C.H., Bundlie, S.R., Ettinger, M.G., Mahowald, M.W., 1986. Chronic behavioral disorders of human REM sleep: a new category of parasomnia. Sleep 9, 293–308. doi:10.1093/sleep/9.2.293.

Schmidt, M.A., Engelhorn, T., Marxreiter, F., Winkler, J., Lang, S., Kloska, S., Goelitz, P., Doerfler, A., 2017. Ultra high-field SWI of the substantia nigra at 7T: reliability and consistency of the swallow-tail sign. BMC Neurol. 17, 1–6. doi:10.1186/s12883-017-0975-2.

Schofield, M.A., Zhu, Y., 2003. Fast phase unwrapping algorithm for interferometric applications. Opt. Lett. 28, 1194–1196. doi:10.1364/OL.28.001194.

Schweser, F., Deistung, A., Lehr, B.W., Reichenbach, J.R., 2011. Quantitative imaging of intrinsic magnetic tissue properties using MRI signal phase: an approach to in vivo brain iron metabolism? Neuroimage 54, 2789–2807. doi:10.1016/j.neuroimage.2010.10.070.

Sian-Hülsmann, J., Mandel, S., Youdim, M.B.H., Riederer, P., 2011. The relevance of iron in the pathogenesis of Parkinson's disease. J. Neurochem. 118, 939–957. doi:10.1111/J.1471-4159.2010.07132.X.

Smith, S.M., 2002. Fast robust automated brain extraction. Hum. Brain Mapp. 17, 143–155. doi:10.1002/hbm.10062.

Sofic, E., Paulus, W., Jellinger, K., Riederer, P., Youdim, M.B.H., 1991. Selective increase of iron in substantia nigra zona compacta of parkinsonian brains. J. Neurochem. 56, 978–982. doi:10.1111/J.1471-4159.1991.TB02017.X.

Spillantini, M.G., Crowther, R.A., Jakes, R., Hasegawa, M., Goedert, M., 1998. alpha-synuclein in filamentous inclusions of Lewy bodies from Parkinson's disease and dementia with lewy bodies. Proc. Natl. Acad. Sci. U. S. A. 95, 6469–6473. doi:10.1073/pnas.95.11.6469.

Sun, H., Walsh, A.J., Lebel, R.M., Blevins, G., Catz, I., Lu, J.Q., Johnson, E.S., Emery, D.J., Warren, K.G., Wilman, A.H., 2015. Validation of quantitative susceptibility mapping with Perls' iron staining for subcortical gray matter. Neuroimage 105, 486–492. doi:10.1016/j.neuroimage.2014.11.010.

Sun, J., Lai, Z., Ma, J., Gao, L., Chen, M., Chen, J., Fang, J., Fan, Y., Bao, Y., Zhang, D., Chan, P., Yang, Q., Ye, C., Wu, T., Ma, T., 2020. Quantitative evaluation of iron content in idiopathic rapid eye movement sleep behavior disorder. Mov. Disord. 35, 478–485. doi:10.1002/mds.27929.

Takahashi, H., Watanabe, Y., Tanaka, H., Mihara, M., Mochizuki, H., Liu, T., Wang, Y., Tomiyama, N., 2018a. Quantifying changes in nigrosomes using quantitative susceptibility mapping and neuromelanin imaging for the diagnosis of early-stage Parkinson's disease. Br. J. Radiol. 91. doi:10.1259/bjr.20180037.

Takahashi, H., Watanabe, Y., Tanaka, H., Mihara, M., Mochizuki, H., Takahashi, K., Yamamoto, K., Liu, T., Wang, Y., Tomiyama, N., 2018b. Comprehensive MRI quantification of the substantia nigra pars compacta in Parkinson's disease. Eur. J. Radiol. 109, 48–56. doi:10.1016/j.ejrad.2018.06.024.

Xuan, M., Guan, X., Gu, Q., Shen, Z., Yu, X., Qiu, T., Luo, X., Song, R., Jiaerken, Y., Xu, X., Huang, P., Luo, W., Zhang, M., 2017. Different iron deposition patterns in early- and middle-late-onset Parkinson's disease. Park. Relat. Disord. 44, 23–27. doi:10.1016/j.parkreldis.2017.08.013.

Yao, C.W., Saha-Chaudhuri, P., Zolfaghari, S., Pelletier, A., Postuma, R.B., 2021. Phenoconversion from possible REM sleep behavior to parkinsonism in the population-based CLSA. Mov. Disord. doi:10.1002/mds.28571.

Youdim, M.B.H., Riederer, P., 1993. The role of iron in senescence of dopaminergic neurons in Parkinson's disease. J. Neural Transm. Suppl. 40, 57–67.

Zecca, L., Gallorini, M., Schünemann, V., Trautwein, A.X., Gerlach, M., Riederer, P., Vezzoni, P., Tampellini, D., 2001. Iron, neuromelanin and ferritin content in the substantia nigra of normal subjects at different ages: consequences for iron storage and neurodegenerative processes. J. Neurochem. 76, 1766–1773. doi:10.1046/J.1471-4159.2001.00186.X.

Zhang, X., Chai, C., Ghassaban, K., Ye, J., Huang, Y., Zhang, T., Wu, W., Zhu, J., Zhang, X., Haacke, E.M., Wang, Z., Xue, R., Xia, S., 2021. Assessing brain iron and volume of subcortical nuclei in idiopathic rapid eye movement sleep behavior disorder. Sleep doi:10.1093/sleep/zsab131.

Zhang, Y., Yang, M., Wang, F., Chen, Y., Liu, R., Zhang, Z., Jiang, Z., 2020. Histogram analysis of quantitative susceptibility mapping for the diagnosis of Parkinson's disease. Acad. Radiol. doi:10.1016/j.acra.2020.10.027.